Osteoarthritis and Cartilage 23 (2015) 1613–1621

Osteoarthritis and Cartilage

Determining collagen distribution in articular cartilage using contrast-enhanced micro-computed tomography

H.J. Nieminen † ‡ *, T. Ylitalo † ‡ [a], S. Karhula ‡ [a], J.-P. Suuronen †, S. Kauppinen ‡ §, R. Serimaa †, E. Hæggström †, K.P.H. Pritzker ||, M. Valkealahti #, P. Lehenkari § ¶ #, M. Finnilä ‡ §, S. Saarakkala ‡ § ††

† *Department of Physics, University of Helsinki, Helsinki, Finland*
‡ *Research Center Group for Medical Imaging, Physics and Technology, Faculty of Medicine, University of Oulu, Oulu, Finland*
§ *Medical Research Center Oulu, Oulu University Hospital and University of Oulu, Finland*
|| *Department of Laboratory Medicine and Pathobiology, University of Toronto and Mount Sinai Hospital, Toronto, Canada*
¶ *Department of Anatomy and Cell Biology, University of Oulu, Finland*
# *Department of Surgery and Intensive Care, University of Oulu and Oulu University Hospital, Finland*
†† *Department of Diagnostic Radiology, Oulu University Hospital, Oulu, Finland*

ARTICLE INFO

Article history:
Received 26 May 2014
Accepted 12 May 2015

Keywords:
Osteoarthritis
Imaging
Collagen
X-ray
Tomography
Articular cartilage

SUMMARY

Objective: Collagen distribution within articular cartilage (AC) is typically evaluated from histological sections, e.g., using collagen staining and light microscopy (LM). Unfortunately, all techniques based on histological sections are time-consuming, destructive, and without extraordinary effort, limited to two dimensions. This study investigates whether phosphotungstic acid (PTA) and phosphomolybdic acid (PMA), two collagen-specific markers and X-ray absorbers, could (1) produce contrast for AC X-ray imaging or (2) be used to detect collagen distribution within AC.
Method: We labeled equine AC samples with PTA or PMA and imaged them with micro-computed tomography (micro-CT) at pre-defined time points 0, 18, 36, 54, 72, 90, 180, 270 h during staining. The micro-CT image intensity was compared with collagen distributions obtained with a reference technique, i.e., Fourier-transform infrared imaging (FTIRI). The labeling time and contrast agent producing highest association (Pearson correlation, Bland–Altman analysis) between FTIRI collagen distribution and micro-CT -determined PTA distribution was selected for human AC.
Results: Both, PTA and PMA labeling permitted visualization of AC features using micro-CT in non-calcified cartilage. After labeling the samples for 36 h in PTA, the spatial distribution of X-ray attenuation correlated highly with the collagen distribution determined by FTIRI in both equine (mean ± S.D. of the Pearson correlation coefficients, $r = 0.96 \pm 0.03$, $n = 12$) and human AC ($r = 0.82 \pm 0.15$, $n = 4$).
Conclusions: PTA-induced X-ray attenuation is a potential marker for non-destructive detection of AC collagen distributions in 3D. This approach opens new possibilities in development of non-destructive 3D histopathological techniques for characterization of OA.

Introduction

To better understand osteoarthritis (OA) greater knowledge about the structural and compositional changes in articular cartilage (AC) with progression of OA is required. Histopathological evaluation is a standard *in vitro* approach to detect changes in osteochondral tissue morphology and related OA stage. Progressing OA alters water, proteoglycan (PG), and collagen content and distribution in AC, as well as size, distribution, orientation, and density

* Address correspondence and reprint requests to: H.J. Nieminen, Department of Physics, University of Helsinki, POB 64, 00014 Helsinki, Finland. Tel: 358-50-3389932.
E-mail addresses: heikki.nieminen@helsinki.fi (H.J. Nieminen), tuomo.ylitalo@helsinki.fi (T. Ylitalo), sakari.karhula@oulu.fi (S. Karhula), jussi-petteri.suuronen@helsinki.fi (J.-P. Suuronen), sami.kauppinen@oulu.fi (S. Kauppinen), ritva.serimaa@helsinki.fi (R. Serimaa), edward.haeggstrom@helsinki.fi (E. Hæggström), kenpritzker@gmail.com (K.P.H. Pritzker), maarit.valkealahti@ppshp.fi (M. Valkealahti), petri.lehenkari@oulu.fi (P. Lehenkari), mikko.finnila@oulu.fi (M. Finnilä), simo.saarakkala@oulu.fi (S. Saarakkala).
[a] Equal contribution.

http://dx.doi.org/10.1016/j.joca.2015.05.004

of chondrocytes[1–3]. The collagen network, which is important for the biomechanics of AC[4,5], is disrupted in OA. This is evident as superficial fibrillation, clefts, and collagen condensation around chondrons[6]. The degeneration can lead to tissue failure and cell death[7] particularly at the transitional zone. It is unclear whether this kind of degeneration induces apoptosis[8,9].

The standard technique to determine collagen distribution in AC is histological sectioning and subsequent staining of the collagen distribution in thin (ca. 5 μm thick) section. Commonly, sections are stained by using collagen labels such as phosphotungstic acid (PTA) or phosphomolybdic acid (PMA)[10]. Another option is to image the collagen within the slice using a label-free approach such as Polarized LM[11], Autofluorescence[12] or FTIRI[13,14]. All section-based techniques are time-consuming and destructive since they involve sample preparation such as, fixation, de-calcification, and cutting of histological sections. 3D reconstruction from serial sections is impractical. Currently, one can study 3D distribution of collagen using contrast-enhanced MRI[15], but MRI lacks the resolution to visualize tissue constructs, e.g., cells, in histologically relevant detail.

There are non-destructive techniques to detect PG distribution in AC using micro-CT and contrast agents such as Hexabrix[16], CA4+/CA1+[17], sodium iodide[18], tantalum oxide nanoparticles[19] and gadopentetate[20]. However, no corresponding methods to detect collagen distribution in the AC volume exist in the literature. In this study, we investigated: (1) whether PTA and PMA can penetrate the AC matrix and label collagen for micro-CT imaging, and (2) if these contrast agents can serve as markers to reveal the spatial distribution of collagen in AC. After first verifying the suitability of the technique with equine AC, we aimed to demonstrate the approach in human AC.

Method

Horse samples

Fresh joints from three horses were obtained from a local slaughterhouse (Veljekset Rönkä Oy, Kemi, Finland). Osteochondral cylinders (n = 12, diameter = 6 mm) were prepared from the anterior medial (AM, n = 3), posterior medial (PM, n = 3), anterior lateral (AL, n = 3) and posterior lateral (PL, n = 3) of proximal phalanxes. Each sample was cut into three pieces [Fig. 1(A)] and subjected to the following procedures: first two pieces (two quarters) were fixed in 4% formalin 5 days (maintenance of tissue structure) and subjected to PTA or PMA staining as described later; the third piece [one half, Fig. 1(A)] was formalin-fixed for 2 days (maintenance of tissue structure), de-calcified with EDTA for 30–60 days (fixes the sample and enhances microtome sectioning), embedded with paraffin (holds the sample during sectioning), and finally sectioned with a microtome (produces 5 μm thick tissue slices). The sections were subjected to FTIRI[7], our reference, to determine the collagen distribution in unstained tissue sections (5 μm thick slices) [Fig. 1(A)].

Human samples

Human osteochondral cylinders (n = 4, diameter = 4.6 mm) were prepared from two patients undergoing total knee arthroplasty; one *tibial* and one *femoral* plug from each of the donors (donor 1: male, age 77 yrs; donor 2: male, age 58 yrs) [Fig. 1(B)]. Institutional ethics approval (PSSHP 78/2013) and patient consents were obtained. Each sample was cut into one half and two quarters [Fig. 1(B)]. Each part (one half and one quarter were used) was fixed, decalcified, and sectioned like the horse samples. The collagen distribution in these unstained sections was assessed by FTIRI and LM using Masson's trichrome staining [Fig. 1(B)][10]. One quarter of the sample was immersed in X-ray contrast agent using the protocol chosen based on the equine tests.

Contrast agent labeling and micro-CT

The horse samples were imaged multiple times with micro-CT: The sample was first imaged at 0 h without markers. Next the sample was immersed in 70% EtOH containing 1% w/v PTA (pH = 2.71) or 1% w/v PMA (pH = 2.35) for 270 h [Fig. 2(A)]. At predefined time points 18, 36, 54, 72, 90, 180 and 270 h the sample was removed from the contrast agent solution, rinsed in 70% ethanol and imaged with micro-CT. The samples were scanned with an *in vivo* micro-CT device (Skyscan 1176, Bruker microCT; settings: 80 kV, 300 mA, 658 projections, exposure 1050 ms/frame, average of 2 frames per projection, 32 min imaging time, 0.5 mm Al filter & 0.038 mm Cu filter, isotropic 8.7 μm voxel side length), while kept in sealed containers with cotton balls moistened with 70% ethanol to prevent drying. The acquired X-ray projections were reconstructed using Skyscan NRecon software (v. 1.6.9, Bruker microCT, Kontich, Belgium) in conjunction with beam hardening and ring artifact corrections. In the resulting images greater attenuation is indicated with brighter contrast similar to conventional X-ray images in which bone appears as brighter contrast and soft tissues appear as darker contrast or with no contrast.

The staining method that most prominently revealed collagen distribution in horse AC (i.e., greatest association between FTIRI collagen distribution and micro-CT -determined PTA distribution as determined by Pearson correlation and Bland–Altman analyses), was selected for the human samples. Following staining, the samples were rinsed in 70% ethanol and scanned with a micro-CT device (Nanotom 180NF, Phoenix X-ray Systems/GE; settings: 80 kV, 100 μA, 1200 projections, exposure 750 ms/frame, average of 7 frames per projection, 2 h 15 min imaging time, no filters, isotropic 3.2 μm voxel side length), while kept in sealed containers with cotton balls moistened with 70% ethanol to prevent drying. The acquired X-ray projections were reconstructed using datos|x reconstruction software (version 1.3.2.11, GE Measurement & Control Solutions/Phoenix X-ray, Fairfield, CT, USA).

Reference methods

The reference collagen distribution was detected from unstained histological sections using FTIRI (Hyperion 3000 FTIRI Microscope, Bruker Inc., Billerica, MA, USA; imaging settings: 2 x 2 binning, 5.4 × 5.4 μm^2 pixel size, 4 cm^{-1} spectral resolution, on average 32 acquisitions per pixel). Collagen content and distribution were directly evaluated from the area under the Amide I peak (1590–1720 cm^{-1}) of the spectrum. This approach has been validated for collagen distribution within normal and osteoarthritic AC histological slices[7,21,22].

Image analysis

The micro-CT image stacks for the horse samples were aligned and re-sliced with the Automated Image Registration software (version 5.3.0, University of California, Berkeley, CA)[23] using a linear rigid body model (6 degrees of freedom) [Fig. 2(B)]. One micro-CT image slice (8.7 μm thickness) per sample was analyzed. The image slice was chosen close to the location from which the histologic section was prepared. The same image location was used for the image sets obtained at all time points. The AC surface, tidemark, and AC-bone interface were manually segmented in the FTIRI and micro-CT images (Fig. 3). The interfaces were then straightened, i.e., each column of the image matrix was normalized (followed by

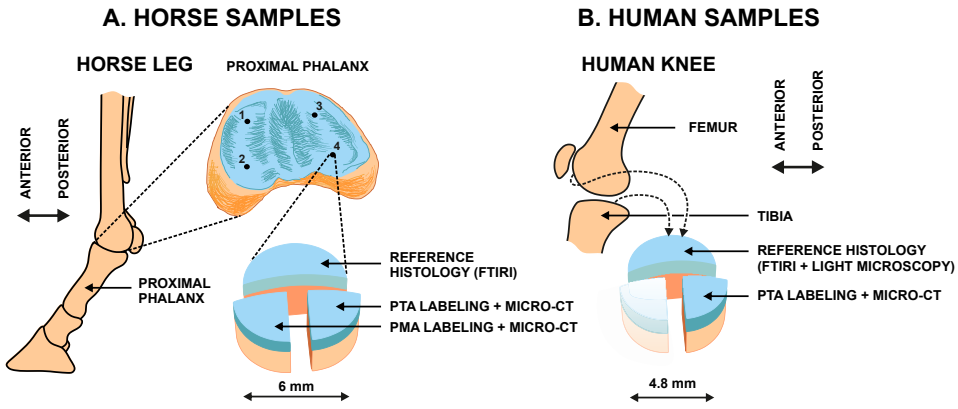

Fig. 1. A. Horse samples ($n = 12$) were collected from proximal phalanxes of three joints from three animals. One half of the osteochondral cylinder was subjected to FTIRI and each of the remaining quarters were subjected to PTA or PMA labeling followed by micro-CT imaging. B. Human samples ($n = 4$) were prepared from knees of two donors undergoing total knee arthroplasty (TKA). Two osteochondral cylinders were obtained from each knee, one from the *tibial* and one from the *femoral* side. One half of the cylinder was subjected to reference histology (FTIRI and Masson staining + LM) and one quarter was subjected to PTA labeling followed by micro-CT.

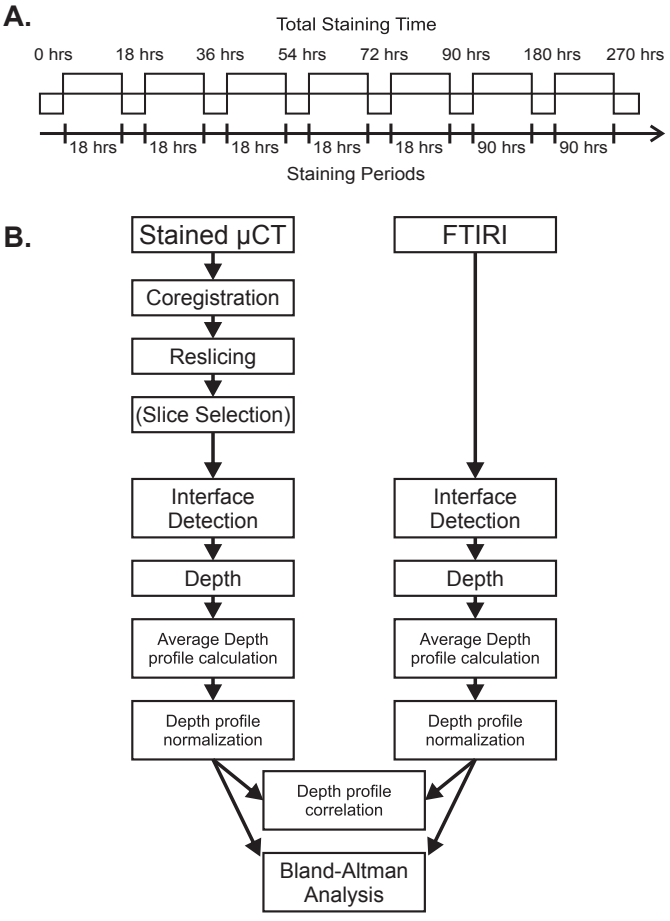

Fig. 2. A. Staining protocol for equine AC. The horse samples ($n = 12$ obtained from three animals) were labeled with PTA or PMA for 270 h. Micro-CT images were acquired at pre-defined time intervals (0, 18, 36, 54, 72, 90, 180, 270 h). B. Schematic for image analysis procedure. The images obtained with FTIRI or micro-CT were manually segmented for AC surface, tidemark, and AC-subchondral bone interface. The images were straightened by linear interpolation and were horizontally averaged to produce the depth-wise image intensity profile. The FTIRI image intensity represented collagen whereas the micro-CT image intensity with PTA or PMA marker was hypothesized to represent collagen. Depth-wise image intensities were compared by means of Pearson correlation analysis, Bland–Altman analysis (equine AC), and Pearson correlation analysis (equine and human AC).

linear interpolation) to cartilage thickness so that zero depth represented the AC surface, 0.72 the tidemark, and 1 the AC-bone interface (0.72 corresponds to the average depth of the tidemark in the normalized image); this resulted in a micro-CT image in which the AC surface, tidemark, and AC-bone interface were all horizontally flat (Fig. 3). Subsequently, a horizontal average (±S.D.) was used to produce the X-ray attenuation profile as a function of AC depth. The same procedure with horizontal averaging was applied to the FTIR Amide I absorption image obtained from the tissue section excised adjacent to the micro-CT sample. To permit qualitative comparison of the collagen profiles, the intensity values of the micro-CT and FTIRI images were also normalized. Image analyses were conducted in a similar manner as with the human samples, but only at the time point 36 h.

For horse AC samples, the comparison between X-ray attenuation and FTIRI intensities was limited to the region between the AC surface and the tidemark due to poor contrast agent penetration into the calcified cartilage. The maximum distance between FTIRI and micro-CT image slices was 4 mm or 2 mm in equine and human AC, respectively. These obtained profiles were compared by Pearson correlation and Bland–Altman analyses (custom-made Matlab program; Matlab 2013a, version 8.1.0.604, MathWorks Inc., Natick, MA, USA) in the horse samples to determine the time required to label the collagen. For human AC samples, Pearson correlation analyses were applied to compare X-ray attenuation and FTIRI intensities.

Results

In the horse samples, micro-CT images showed increasing X-ray attenuation between the superficial AC and the tidemark from the 36 h time point onwards (Figs. 3 and 4). In addition, increased intensity was observed at the AC surface and slightly decreased intensity in the middle zone (Figs. 3 and 4). Staining prolonged for more than 36 h produced excess X-ray attenuation at the tidemark and the superficial AC in the PMA-stained samples. A similar phenomenon, but exhibiting a smaller effect, was detectable in PTA-stained samples when the staining time exceeded 54 h.

In the horse samples (thickness: 943 ± 86 µm, $n = 12$), the best match (highest Pearson correlation coefficient) between the X-ray attenuation profile and the FTIRI collagen profile was observed at 36 h ($r = 0.96 \pm 0.03$, $n = 12$) and 54 h ($r = 0.96 \pm 0.03$, $n = 12$) using PTA staining (Table I). Bland–Altman analysis revealed that the best

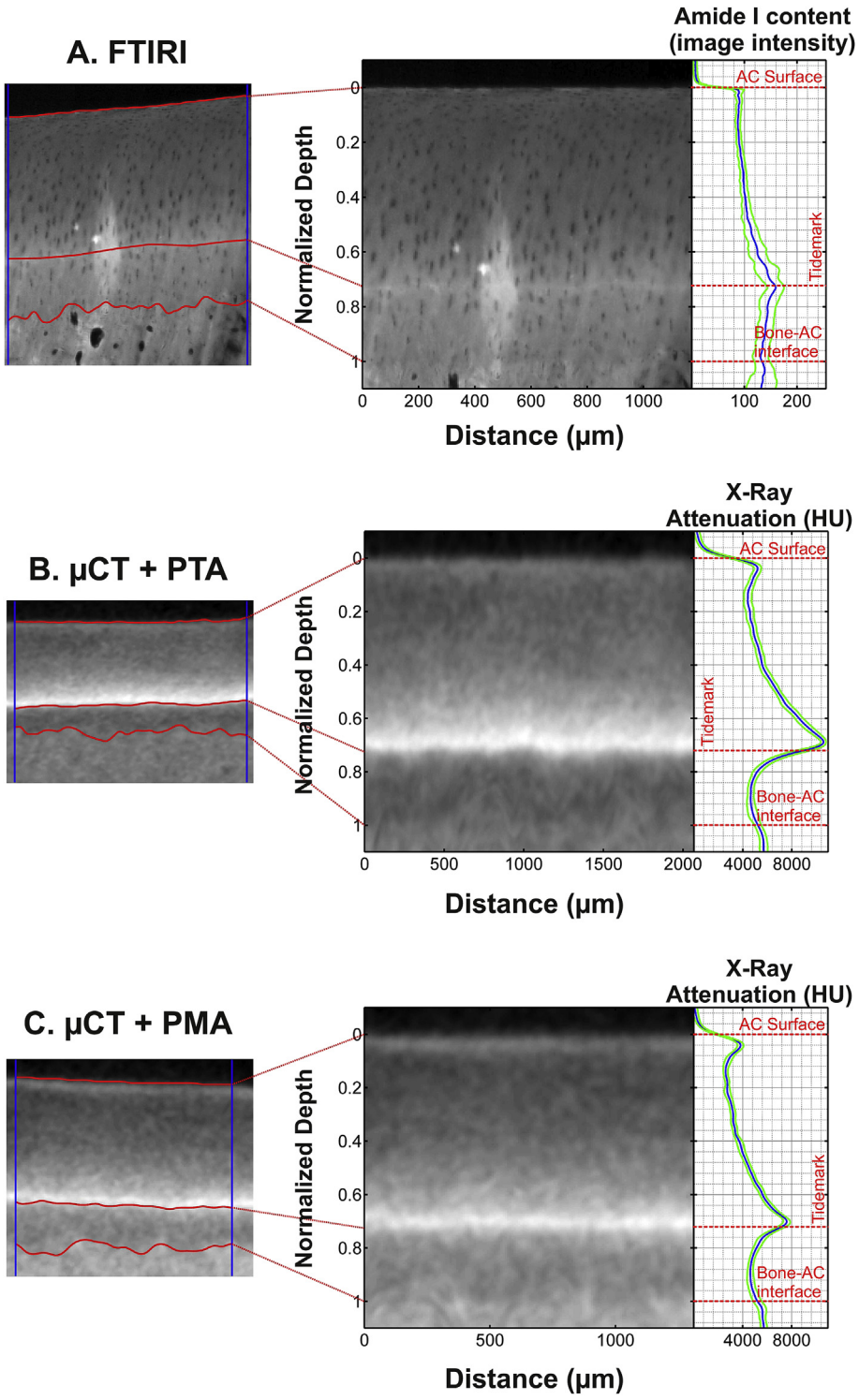

Fig. 3. Examples of images (left) obtained from horse AC using FTIRI (A) of unstained sections and micro-CT following PTA (B) or PMA (C) labeling. The center column demonstrates the images after normalizing by AC thickness whereas the right hand column demonstrates the depth-wise image intensity profiles (horizontal average ± S.D.). The depth-wise contrast profile in the micro-CT image is in line with FTIRI profile; i.e., the very superficial AC and deep AC is rich in collagen compared to the middle AC. The FITRI sample (A) demonstrates a bright irregular area at the center of the region of interest due to a typical artifact seen when imaging tissue sections with FTIRI (the section is slightly detached from the glass slide). The analyses were restricted between the vertical blue lines. The micro-CT images presented here were acquired at 36 h.

correspondence between FTIRI-detected collagen and micro-CT -detected PTA was observed at time points 36 h and 54 h. In these sets 95% of micro-CT image intensity data points differed from corresponding FTIRI values by less than 18.1% (Fig. 5). Staining with PMA produced slightly lower correlation with the FTIRI collagen profile (Table I). The highest correlations were observed at 18 h ($r = 0.93 \pm 0.07$, $n = 12$) and 36 h ($r = 0.90 \pm 0.14$, $n = 12$) (Table I). Based on the Bland–Altman analysis, the best

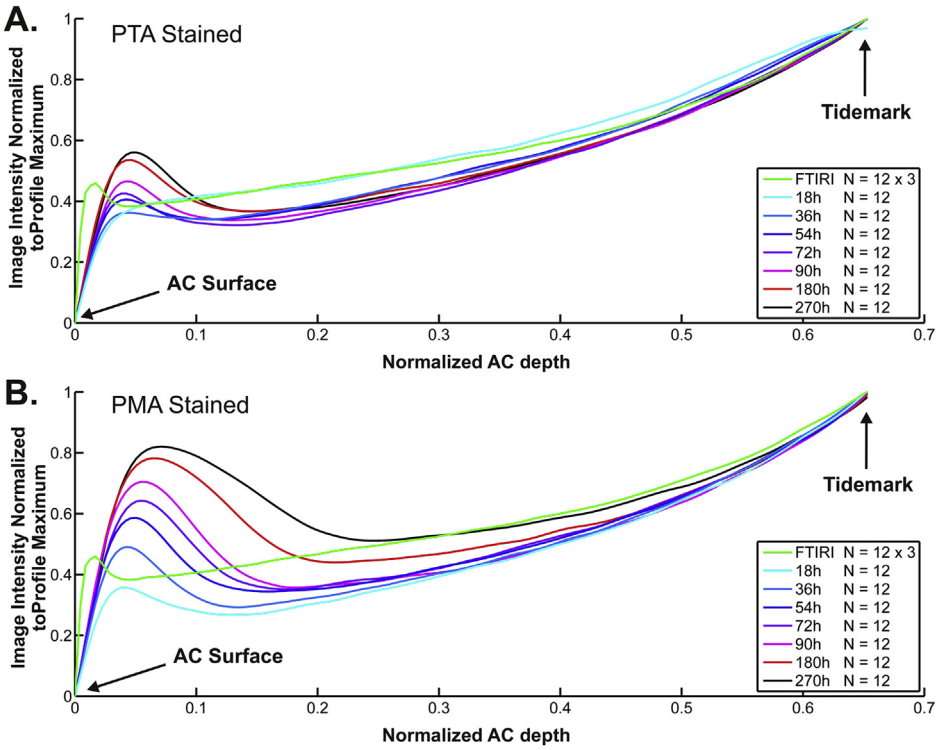

Fig. 4. Average depth-wise image intensities for equine AC obtained with micro-CT at predefined time points of collagen-labeling. A. Average micro-CT image intensity ($n = 12$ for each time point) following (PTA) staining corresponded with the depth-wise collagen content obtained with the reference FTIRI technique ($n = 12$). B. Average micro-CT image intensity ($n = 12$ for each time point) following (PMA) partially corresponded with the depth-wise collagen content obtained with FTIRI. The best correspondence between micro-CT and FTIRI profiles, i.e., highest Pearson correlation and smallest difference in Bland–Altman analysis (Table I, Fig. 5), was obtained with 36 h or 54 h immersion in PTA solution. The 36 h labeling time was selected as the labeling time for human AC. The 12 samples were obtained from three animals.

correspondence of FTIRI-detected collagen and micro-CT -detected PMA was at time points 18 h and 72 h. In these sets 95% of micro-CT image data points deviated by less than ±25.1% from the respective data points acquired with FTIRI. Based on correlation and the Bland–Altman analyses, PTA was selected as marker for human AC and 36 h as staining time.

In human AC (thickness: 2154 ± 934 μm, $n = 4$), PTA provided X-ray contrast to the extracellular collagen matrix (Fig. 6). In three human samples a non-enhancing region (width 454–1531 μm, height 84–394 μm) was observed adjacent to the tidemark or subchondral bone interface. Qualitatively, PTA and FTIRI images resembled each other by exhibiting high collagen content in the superficial and deep cartilage, lower collagen in middle region, and appearance of chondrons (Fig. 6). The correlation between the FTIRI-detected collagen and micro-CT -detected PTA distributions ($n = 4$) were $r = 0.86$, 0.61, 0.83 and 0.96 (Fig. 6). The PTA contrast permitted 3D visualization of the entire AC sample including the AC surface (Fig. 7).

Discussion

Both staining agents (PTA and PMA) provided contrast to the horse AC matrix as compared to the AC matrix at 0 h without staining. PTA staining also provided X-ray contrast to the human AC tissue. The X-ray attenuation was high in superficial and deep cartilage, and lower in the middle zone and inside the chondrons. The depth-wise contrast profile in the micro-CT image agrees with FTIRI and our previous report on the collagen distribution in AC[7], where the very superficial AC and deep AC is rich in collagen compared to the middle AC. Micro-CT visualized the tidemark clearly (Fig. 6); however, it appeared as if depth-wise PTA penetration was significantly hindered when the penetration front met the tidemark. The chondrons were visible in human AC and but not in horse AC due to the following reasons: (1) the human AC samples with degeneration contained hypertrophic chondrocytes in large clusters; (2) the X-ray resolution was higher in the system used to image human AC.

FTIRI images (Amide I peak) indicating collagen content distribution in tissue sections resembled the X-ray attenuation images in the region from superficial AC to the tidemark in human AC (Fig. 6). The Amide I peak and PTA-induced X-ray attenuation profiles were similar in equine cartilage with except for at the very superficial AC (the superficial layer corresponding to 11% of AC thickness, Figs. 3–5). This was further supported by the Bland–Altman analyses. The FTIRI and micro-CT contrasts differed in the region with calcified cartilage. This is potentially due to slow or lack of PTA penetration into calcified cartilage, whose permeability is lower than that of the AC matrix[24].

In horse samples, best correspondence between X-ray attenuation and FTIRI intensity from all samples, i.e., the highest average correlation and smallest error in Bland–Altman analyses, was recorded with 36 h and 54 h PTA staining. This indicates that 36 h is sufficient staining time for visualization of collagen in equine AC. On the contrary, the PMA staining appeared to induce excess X-ray attenuation near the AC surface and the tidemark. This leads to weaker resemblance between the X-ray attenuation and FTIRI intensity. Consequently, PMA was not chosen for further experiments. Horse AC was considered an appropriate

Table I
Pearson correlation coefficients (micro-CT vs FTIRI) of depth-wise image intensities at different time points (18, 36, 54, 72, 90, 180, 270 h) of (PTA, top) and (PMA, bottom) labeling of horse AC. Correlation coefficients 0.95 or greater are in green. The highest correlations were obtained with 36 h and 54 h immersion in PTA

Correlations Between FTIRI and PTA Stained Cartilage

	18 h	36 h	54 h	72 h	90 h	180 h	270 h
Sample 1	0.99	0.98	0.97	0.97	0.94	0.94	0.88
Sample 2	0.91	0.94	0.93	0.90	0.85	0.86	0.80
Sample 3	0.97	0.98	0.97	0.98	0.94	0.97	0.94
Sample 4	0.65	0.95	0.95	0.94	0.94	0.91	0.92
Sample 5	0.99	0.99	0.99	0.97	0.96	0.94	0.95
Sample 6	0.98	0.97	0.96	0.92	0.93	0.86	0.90
Sample 7	0.98	0.98	0.98	0.98	0.97	0.97	0.94
Sample 8	0.80	0.95	0.95	0.96	0.96	0.97	0.97
Sample 9	0.90	0.94	0.91	0.95	0.93	0.92	0.88
Sample 10	0.99	0.98	0.97	0.93	0.93	0.89	0.87
Sample 11	0.95	0.98	0.98	0.95	0.95	0.94	0.91
Sample 12	0.89	0.89	0.90	0.92	0.88	0.91	0.87
Mean	0.92	0.96	0.96	0.95	0.93	0.92	0.90
SD	0.10	0.03	0.03	0.03	0.04	0.04	0.05

Correlations Between FTIRI and PMA Stained Cartilage

	18 h	36 h	54 h	72 h	90 h	180 h	270 h
Sample 1	0.97	0.96	0.94	0.93	0.87	0.82	0.79
Sample 2	0.74	0.46	0.33	0.25	-0.09	-0.23	-0.25
Sample 3	0.98	0.95	0.94	0.88	0.74	0.67	0.52
Sample 4	0.98	0.96	0.88	0.88	0.89	0.77	0.65
Sample 5	0.97	0.96	0.94	0.90	0.85	0.80	0.85
Sample 6	0.96	0.94	0.88	0.85	0.77	0.67	0.74
Sample 7	0.98	0.96	0.94	0.91	0.87	0.74	0.66
Sample 8	0.92	0.97	0.88	0.75	0.79	0.63	0.38
Sample 9	0.94	0.94	0.94	0.92	0.90	0.74	0.61
Sample 10	0.95	0.81	0.77	0.77	0.65	0.60	0.48
Sample 11	0.96	0.96	0.93	0.90	0.86	0.81	0.67
Sample 12	0.85	0.88	0.70	0.80	0.67	0.49	0.31
Mean	0.93	0.90	0.84	0.81	0.73	0.63	0.54
SD	0.07	0.14	0.18	0.19	0.27	0.29	0.30

tissue model for the labeling experiments, because it is similar to human AC with regards to thickness, structure, and composition[25,26].

In human samples, the Pearson correlation analyses suggested that the 36 h staining time is suitable to detect collagen distribution. A lower correlation ($r = 0.61$) in one sample [Fig. 6(B)] may be explained by the fact that chondrons, which have low image contrast, occupied a relatively large volume in this sample. It is possible that prolonged staining due to long penetration distances may be required for human AC samples of this size (AC width 2 mm, height 2.2 ± 0.9 mm). Furthermore, it is noteworthy that the observed non-enhancing region in three human samples did not affect our analysis since we chose the micro-CT image slice from the sample boundary (400–800 μm distance) close to the FTIRI sample.

Earlier literature suggests that PTA and PMA staining relies mainly on ionic bonds with collagen[27,28]. This mechanism is exploited in conventional histological staining techniques such as Masson's trichrome staining[10]. Due to high negative charge of PMA/PTA molecules, the repulsive forces from negatively charged PGs may affect the staining. However, based on our recent results (unpublished), depletion of PGs does not significantly affect PTA-induced X-ray attenuation in bovine AC. On the contrary, removing collagen with collagenase remarkably decreased the PTA-induced X-ray attenuation. While there may be high correlation between PG and collagen contents, the proposed technique appears to be specific to collagen and not affected by PG.

The applied PTA staining permitted 3D reconstruction of the entire osteochondral sample including the AC surface (Fig. 7). This allowed the evaluation of superficial morphology, e.g., the existence of clefts and fibrillation (See supplemental Videos 1 and 2). Visualizing superficial fibrillation is important, because this early pathological change in OA, is scored in conventional histopathological grading[1]. Moreover, the surface fibrillation is associated with the biomechanical properties of the cartilage[3]. Albeit the micro-CT does not resolve collagen bundles within the AC matrix, indirect interpretations could potentially be made based on the alignment of the extracellular matrix.

Supplementary videos related to this article can be found at http://dx.doi.org/10.1016/j.joca.2015.05.004.

There are limitations to the present study. The sample population is small, i.e., the 12 horse samples were from 3 animals and the 4 human samples were from 2 individuals introducing potential bias arising from multiple observations from single individuals[29]. While correlation analysis was applied to identify the proper PTA staining time, the results may potentially be affected by collinearity of the collagen profiles determined with the different techniques. Therefore, validation with samples from a large patient population would be needed to generalize the association between the micro-CT –determined and the FTIRI-determined collagen distributions. The resolution of the micro-CT device used with horse samples reduces the accuracy of the results at superficial cartilage. The core diameters were different in

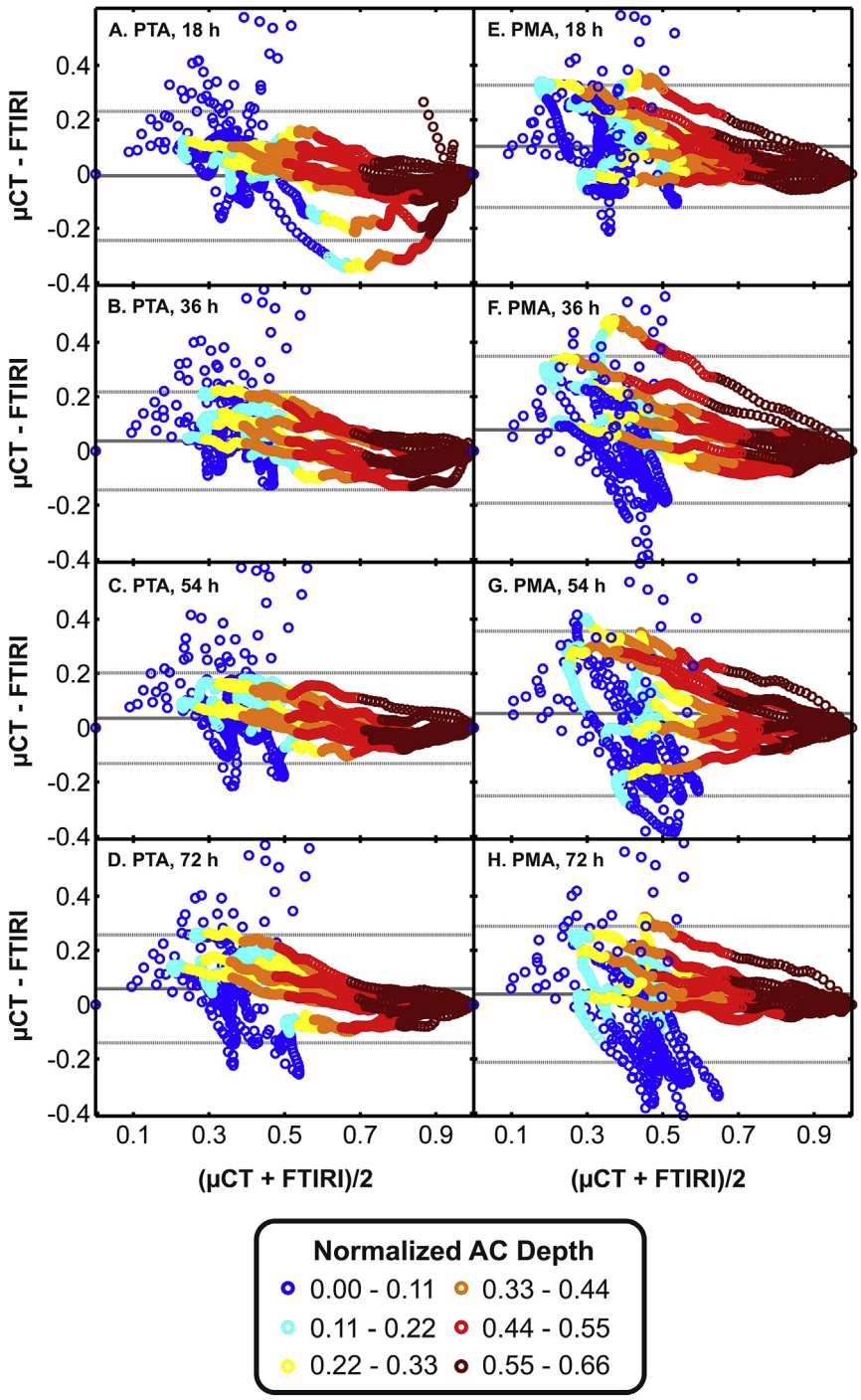

Fig. 5. Bland–Altman comparison of normalized image intensity profiles obtained with micro-CT or FTIRI in horse samples. The left and right column represents data obtained following PTA (A–D) or PMA (E–H) at immersion time points 18, 36, 54 and 72 h. Best correspondence, i.e., smallest difference, between micro-CT and FTIRI profiles were obtained following PTA labeling for 36 or 54 h. The color codes in the legend represent the relative depth of data points from the AC surface. Color coding revealed that the micro-CT vs FTIRI profiles differed most at superficial AC.

human AC as compared to equine AC in order to achieve high angular magnification for micro-CT imaging of human AC. The use of PTA staining is limited to *ex vivo* use because of the acidity. Furthermore, PTA stains collagen in general rather than specific collagen type. Despite these limitations there are several advantages associated with the proposed technique: Since PTA stains collagen it provides similar information about collagen distribution as conventional histology (e.g., Masson's trichrome staining and LM), but in 3D and full thickness AC. Only laborious alternatives, such as slice-by-slice characterization of a tissue volume using conventional histology can provide comparable details as the proposed PTA-enhanced micro-CT technique. Another advantage of this technique over conventional histology is the detail in visualizing the tidemark.

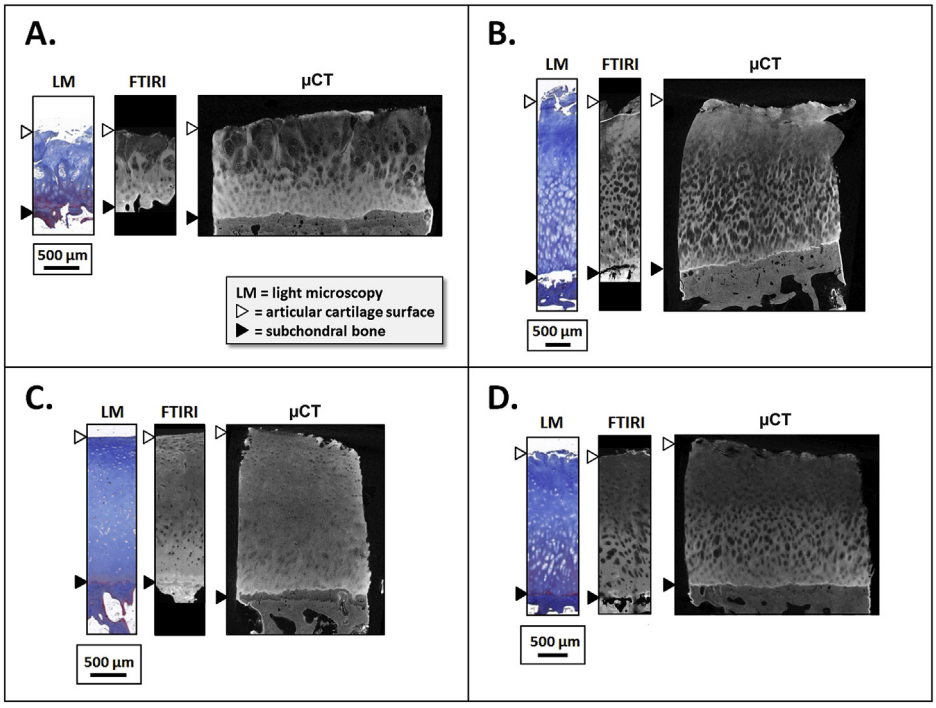

Fig. 6. Micro-CT images of human AC samples (A–D) showed similar features as the FTIRI images: (i) with both micro-CT and FTIRI, high image intensities were observed at superficial and the extra-cellular matrix of deep AC; (ii) lower image intensity was observed at the extra-cellular matrix of middle zone AC and in chondrons throughout AC. The Pearson correlation coefficients for depth-wise image intensities (FTIRI vs micro-CT) were 0.86 (A), 0.61 (B), 0.83 (C) and 0.96 (D) suggesting that depth-wise micro-CT image intensity following PTA labeling may be associated with collagen content. By comparing the blue contrast in Masson's trichrome stained LM images with respective micro-CT and FTIRI images one can qualitatively detect the similarities in their information regarding collagen content: strong and faint blue contrast in LM is observed as strong and faint brightness in FTIRI and micro-CT. The brightness and contrast in the FTIRI and micro-CT images were separately adjusted for demonstration purposes only, but not applied to data subjected for correlation analyses.

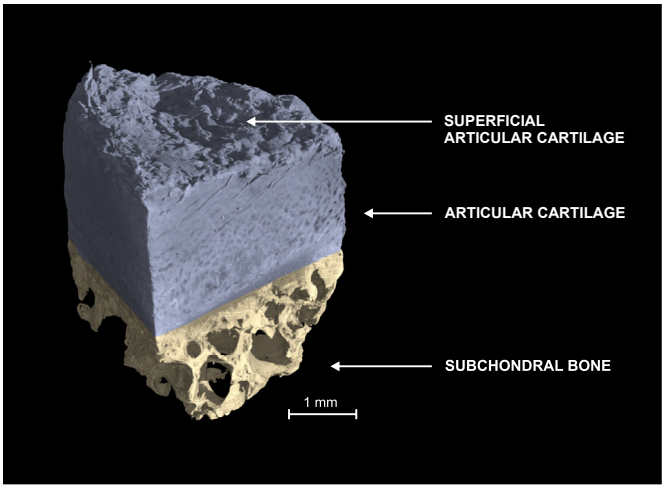

Fig. 7. 3D reconstruction of a human sample subjected PTA labeling and micro-CT. PTA produced strong contrast allowing 3D visualization of the superficial collagen degeneration.

Conclusions

To our understanding, this study is the first contribution towards characterizing collagen distribution non-destructively within the entire AC volume. Since the proposed technique produces contrast variation in the AC tissue matrix, it may open new possibilities for development of CT-based non-destructive 3D-histopathological techniques to assess cartilage degeneration, injury and repair.

Author contributions

HJN, TY, SK1, SK2, RS, EH, KPHP, MF and SS contributed to the conception and design of the study. HJN, TY, SK1, J-PS., SK2, KPHP, MV, PL, MF, and SS participated in acquisition and analysis of the data. All authors contributed to interpreting the data, drafting or revising the manuscript, and have approved the submitted version of the manuscript.

Role of the funding source

Funding sources are not associated with the scientific contents of the study.

Competing interests

- Dr HJ Nieminen reports no conflicts of interest.
- Mr T Ylitalo reports no conflicts of interest.
- Mr S Karhula reports no conflicts of interest.
- Mr JP Suuronen reports no conflicts of interest.
- Mr S Kauppinen reports no conflicts of interest.
- Prof R Serimaa reports no conflicts of interest.
- Prof E Hæggström reports no conflicts of interest.
- Prof KPH Pritzker reports no conflicts of interest.
- Dr M Valkealahti reports no conflicts of interest.
- Prof P Lehenkari reports no conflicts of interest.
- Dr M Finnilä reports no conflicts of interest.
- Dr S Saarakkala reports no conflicts of interest.

Acknowledgments

The financial support from the Academy of Finland (grants no. 268378, 273571 and 253579); Sigrid Juselius Foundation; European Research Council under the European Union's Seventh Framework Programme (FP/2007-2013)/ERC Grant Agreement no. 336267; and the strategic funding of the University of Oulu are acknowledged. We thank Mr. Risto Bloigu, M.Sc., the professional statistician of Faculty of Medicine, University of Oulu, Finland, for statistical expertise.

We thank Veljekset Rönkä Oy (Kemi, Finland) for providing the horse joints.

References

1. Pritzker KPH, Gay S, Jimenez SA, Ostergaard K, Pelletier JP, Revell PA, *et al*. Osteoarthritis cartilage histopathology: grading and staging. Osteoarthritis Cartilage 2006;14:13–29.
2. Jones WR, Ting-Beall HP, Lee GM, Kelley SS, Hochmuth RM, Guilak F. Alterations in the Young's modulus and volumetric properties of chondrocytes isolated from normal and osteoarthritic human cartilage. J Biomech 1999;32:119–27.
3. Temple-Wong MM, Bae WC, Chen MQ, Bugbee WD, Amiel D, Coutts RD, *et al*. Biomechanical, structural, and biochemical indices of degenerative and osteoarthritic deterioration of adult human articular cartilage of the femoral condyle. Osteoarthritis Cartilage 2009;17:1469–76.
4. Bi X, Yang X, Bostrom MPG, Camacho NP. Fourier transform infrared imaging spectroscopy investigations in the pathogenesis and repair of cartilage. Biochim Biophys Acta Biomembr 2006;1758:934–41.
5. Guilak F, Jones WR, Ting-Beall HP, Lee GM. The deformation behavior and mechanical properties of chondrocytes in articular cartilage. Osteoarthritis Cartilage 1999;7:59–70.
6. Pritzker KPH. Pathology of osteoarthritis. In: Brandt KD, Doherty M, Lohmander LS, Eds. Osteoarthritis. 2nd edn. Oxford: Oxford University Press; 2003.
7. Saarakkala S, Julkunen P, Kiviranta P, Mäkitalo J, Jurvelin JS, Korhonen RK. Depth-wise progression of osteoarthritis in human articular cartilage: investigation of composition, structure and biomechanics. Osteoarthritis Cartilage 2010;18:73–81.
8. Aigner T, Hemmel M, Neureiter D, Gebhard PM, Zeiler G, Kirchner T, *et al*. Apoptotic cell death is not a widespread phenomenon in normal aging and osteoarthritis human articular knee cartilage: a study of proliferation, programmed cell death (apoptosis), and viability of chondrocytes in normal and osteoarthritic human knee cartilage. Arthritis Rheum 2001;44:1304–12.
9. Ewers BJ, Dvoracek-Driksna D, Orth MW, Haut RC. The extent of matrix damage and chondrocyte death in mechanically traumatized articular cartilage explants depends on rate of loading. J Orthop Res 2001;19:779–84.
10. Luna LG. Manual of Histologic Staining Methods; of the Armed Forces Institute of Pathology. New York: Blakiston Division, McGraw-Hill; 1968.
11. Benninghoff A. Form und Bau der Gelenkknorpel in ihren Beziehungen zur Funktion. Z Zellforsch Mik Ana 1925;2:783–862.
12. Gibson GJ, Verner JJ, Nelson FRT, Lin DL. Degradation of the cartilage collagen matrix associated with changes in chondrocytes in osteoarthrosis. Assessment by loss of background fluorescence and immunodetection of matrix components. J Orthop Res 2001;19:33–42.
13. Muyonga J, Cole C, Duodu K. Fourier transform infrared (FTIR) spectroscopic study of acid soluble collagen and gelatin from skins and bones of young and adult Nile perch (*Lates niloticus*). Food Chem 2004;86:325–32.
14. Rieppo L, Saarakkala S, Jurvelin JS, Rieppo J. Optimal variable selection for Fourier transform infrared spectroscopic analysis of articular cartilage composition. J Biomed Opt 2014;19:027003.
15. Chen W, Cormode DP, Vengrenyuk Y, Herranz B, Feig JE, Klink A, *et al*. Collagen-specific peptide conjugated HDL nanoparticles as MRI contrast agent to evaluate compositional changes in atherosclerotic plaque regression. JACC Cardiovasc Imaging 2013;6:373–84.
16. Palmer AW, Guldberg RE, Levenston ME. Analysis of cartilage matrix fixed charge density and three-dimensional morphology via contrast-enhanced microcomputed tomography. Proc Natl Acad Sci USA 2006;103:19255–60.
17. Bansal PN, Joshi NS, Entezari V, Malone BC, Stewart RC, Snyder BD, *et al*. Cationic contrast agents improve quantification of glycosaminoglycan (GAG) content by contrast enhanced CT imaging of cartilage. J Orthop Res 2011;29:704–9.
18. Kokkonen H, Jurvelin J, Tiitu V, Töyräs J. Detection of mechanical injury of articular cartilage using contrast enhanced computed tomography. Osteoarthritis Cartilage 2011;19:295–301.
19. Freedman JD, Lusic H, Snyder BD, Grinstaff MW. Tantalum oxide nanoparticles for the imaging of articular cartilage using X-ray computed tomography: visualization of ex vivo/in vivo murine tibia and ex vivo human index finger cartilage. Angew Chem Int Ed Engl 2014;53:8406–10.
20. Kallioniemi A, Jurvelin J, Nieminen M, Lammi M, Töyräs J. Contrast agent enhanced pQCT of articular cartilage. Phys Med Biol 2007;52:1209.
21. Camacho NP, West P, Torzilli PA, Mendelsohn R. FTIR microscopic imaging of collagen and proteoglycan in bovine cartilage. Biopolymers 2001;62:1–8.
22. Boskey A, Pleshko Camacho N. FT-IR imaging of native and tissue-engineered bone and cartilage. Biomaterials 2007;28:2465–78.
23. Woods RP, Cherry SR, Mazziotta JC. Rapid automated algorithm for aligning and reslicing PET images. J Comput Assist Tomogr 1992;16:620–33.
24. Arkill KP, Winlove CP. Solute transport in the deep and calcified zones of articular cartilage. Osteoarthritis Cartilage 2008;16:708–14.
25. Frisbie DD, Cross MW, McIlwraith CW. A comparative study of articular cartilage thickness in the stifle of animal species used in human pre-clinical studies compared to articular cartilage thickness in the human knee. Vet Comp Orthop Traumatol 2006;19:142–6.
26. Malda J, Benders K, Klein T, De Grauw J, Kik M, Hutmacher D, *et al*. Comparative study of depth-dependent characteristics of equine and human osteochondral tissue from the medial and lateral femoral condyles. Osteoarthritis Cartilage 2012;20:1147–51.
27. Puchtler H, Isler H. The effect of phosphomolybdic acid on the stainability of connective tissues by various dyes. J Histochem Cytochem 1958;6:265–70.
28. Constantine VS, Mowry RW. Selective staining of human dermal collagen. I. An analysis of standard methods. J Invest Dermatol 1968;50:414–8.
29. Bryant D, Havey TC, Roberts R, Guyatt G. How many patients? How many limbs? Analysis of patients or limbs in the orthopaedic literature: a systematic review. J Bone Joint Surg Am 2006;88:41–5.